

Channel-Correlation-Based Access Point Selection and Pilot Power Allocation for Cell-Free Massive MIMO

Saeed Mohammadzadeh, *Member, IEEE*, Rodrigo C. De Lamare, *Fellow Member, IEEE*, Kanapathippillai Cumanan, *Senior Member, IEEE*, and Hien Quoc Ngo, *Fellow, IEEE*.

Abstract—This paper proposes a dynamic access point (AP) selection and pilot power allocation (DAPPA) framework for uplink cell-free massive multiple-input multiple-output (CFmMIMO) systems, aiming to mitigate inter-user interference and improve overall spectral efficiency (SE). A hierarchical correlation-based clustering algorithm is developed to group APs according to their channel correlation, enabling each user to be associated with APs that simultaneously provide strong channel gains and low mutual correlation. This association ensures reliable connectivity, maximizes coherent combining gains, and reduces inter-user interference, while also allowing the number of AP clusters to be adjusted flexibly, without the need to reorganize the network completely. By maintaining links to low-correlated APs, the proposed scheme reduces the need for frequent channel state information (CSI) estimation and minimizes network-wide update overhead. To enhance scalability, a user-capacity constraint per AP is incorporated, preventing hardware overload and alleviating the effects of pilot reuse. Furthermore, an effective pilot power allocation strategy is introduced to boost the signal-to-interference-plus-noise ratio (SINR) during channel training. This is formulated as a weighted sum-rate maximization (WSRM) problem and solved iteratively using a quadratic transform, which enables efficient optimization while ensuring fairness and high-quality service across all users. Numerical results demonstrate that the proposed method delivers significant SE gains, maintains performance in high-density multi-user scenarios, and converges faster than benchmark schemes.

Index Terms—Access point selection, cell-free massive MIMO, scalability, weighted sum-rate maximization.

I. INTRODUCTION

Cell-free massive multiple-input multiple-output (CFmMIMO) systems are a promising technology for future wireless communication networks, offering seamless connectivity and superior service quality to users [1], [2]. In CFmMIMO networks, a large number of distributed access points (APs) collaboratively serve user devices across a wide area without the need for traditional cell boundaries. These APs connect to one or several central processing units (CPUs) via fronthaul links, with the CPUs interconnected through a backhaul network [3]–[5]. CFmMIMO networks offer enhanced spectral and energy efficiency, leveraging benefits like favorable propagation, high macro-diversity, efficient resource allocation, and channel hardening [6]–[8].

S. Mohammadzadeh, R. C. De Lamare, and K. Cumanan are with the School of Physics, Engineering and Technology, University of York. UK. (email: Saeed.mzadeh@ieee.org; rodrigo.delamare@york.ac.uk; kanapathippillai.cumanan@york.ac.uk).

H. N. Ngo is with the School of Electronics, Electrical Engineering and Computer Science, Queen’s University Belfast, (email:hien.ngo@qub.ac.uk).

A. Prior and Related Works

In standard CFmMIMO networks, all APs serve all the users simultaneously [9]. However, in these systems, the required number of channel measurements increases linearly with both the number of APs and users, resulting in substantial channel state information (CSI) signaling overhead and higher signal processing complexity [10]. In reality, a user’s signal power is primarily influenced by a limited number of nearby APs, as path loss increases exponentially with distance. This suggests that coordinating all APs to serve every user jointly is unnecessary. To overcome these challenges, recent approaches assign tailored AP clusters to users, enhancing the scalability of CFmMIMO networks [11]–[23].

In [11], a user-centric overlapped clustering algorithm based on a graph-theoretical framework is proposed. The AP selection in [13] is proposed based on two schemes, utilizing the received power-based selection and the largest-scale fading (LSF)-based approach [24], [25]. In [14], a method was introduced that utilizes a dynamic set of APs to serve each user based on the virtual cell approach and system performance, or large-scale fading [15]. The authors in [16] propose a method in which each AP serves the users within its coverage of some radius. The work in [18] proposed a structured massive access-based pilot assignment strategy that forms groups with users having a minimum intersection of shared serving APs and assigns orthogonal pilots. In [19], the AP selection problem was introduced as a local altruistic game based on its inherent interference relationship. The distance-based AP selection and random-access point selection algorithms are used to choose APs in [20].

In [22], a clustered cell-free network architecture was proposed, where the entire network is divided into non-overlapping sub-networks, each operating independently with cooperative transmission. In [21], an AP selection strategy based on quantum bacterial foraging optimization is proposed, which encodes the connection relationship between APs and users in the form of qubits. Authors in [26] propose a joint pilot assignment scheme based on user clustering and graph coloring, where AP selection is first used to group users, followed by graph-based pilot allocation. The scheme in [27] utilizes a hierarchical clustering algorithm employing the Euclidean distance between the APs to group APs based on the minimax linkage criterion [28], while the deep learning-based version is introduced in [29]. In [30], user clustering is performed using a hierarchical method, while AP selection is based on large-

scale fading decoding and the normalized channel estimation mean square error. In [31], the authors developed a multi-agent reinforcement learning (MARL) algorithm for AP selection and clustering. Each AP is an agent in the MARL algorithm, trained to select which users to serve near-optimally. Recently, clustering based on the sum-rate criterion was reported in [32] and showed enhanced AP clustering.

Moreover, it is well known that to achieve an efficient resource allocation in wireless systems, power control (PC) is crucial, helping to reduce interference [33]–[35], boost performance, and meet quality of service requirements for users in CFmMIMO networks [36], [37]. By optimizing both pilot and data power, spatial diversity in the wireless channel can be better exploited, reducing the impact of pilot contamination, inter-user interference, and noise [38], [39]. However, designing efficient algorithms to manage PC in large-scale CFmMIMO networks remains a complex task, largely due to the intricate nature of the optimization problem and practical constraints such as computational costs and signaling overhead. The works in [40]–[44] explored the impact of pilot and PC in the uplink of cell-based systems. However, the optimization algorithms used in these cellular systems are not directly applicable to cell-free systems. In cell-free systems, each serving AP must estimate the channels to its users using the uplink pilot signal. Moreover, prior work on cell-free systems focused on optimizing data power [2], [45] while assuming either full or fixed power for transmitting pilot signals.

Using a bisection search algorithm, the study in [2] addressed the max-min PC problem in CFmMIMO networks. In [46], an algorithm was introduced using a pilot PC scheme to minimize the maximum channel estimation error among users. It employed the data power allocation strategy from [2] to address a max-min fairness problem, while AP selection was based on the LSF criteria. However, the key challenge with this approach lies in the time-consuming process of finding the maximum LSF values for all users across all APs. In [47], a joint PC method was considered for single-antenna APs, where users have limited total energy. The work in [48] explored a first-order Taylor approximation approach, jointly optimizing pilot and data power using a greedy power algorithm. In user-centric scenarios [49], authors proposed a joint pilot and data PC by combining successive convex approximation and geometric programming (GP). Furthermore, the work in [50] employed a sequential convex approximation algorithm to solve a GP problem for jointly controlling pilot and data power. Moreover, a fractional PC policy for uplink CFmMIMO was presented in [51], which can be fully distributed and uses large-scale quantities. Inspired by weighted minimum mean square error (WMMSE) and fractional programming, the algorithm in [52] proposed a fair power allocation. Deep neural networks (DNNs) were introduced in [53]–[55] to reduce complexity, including convolutional neural network models, distributed DNNs, and graph neural networks for efficient PC optimization with maximum ratio transmission beamforming.

B. Contribution

Motivated by the above discussion, we propose a dynamic AP selection and pilot power allocation schemes to enhance the spectral efficiency (SE) of uplink CFmMIMO systems in this work. We form AP clusters instead of user clusters and then associate users with these clustered APs based on channel correlation. Using a specified linkage criterion, the algorithm builds a dendrogram that shows how clusters merge or split as their number changes. Its key advantage is that adjusting the number of clusters only affects the involved clusters, leaving others unchanged. In contrast, methods like K-means or spectral clustering require reclustering the entire network when the cluster count changes, leading to widespread CSI re-estimation, an undesirable overhead in wireless networks. To address this, we propose an algorithm that efficiently adapts the number of clusters to the network’s current state without requiring a full-scale update. Additionally, our approach relies only on local CSI, which is used for user association, making it a scalable and efficient solution. The primary advantage of the proposed method over traditional techniques lies in its correlation-based clustering approach. This method is designed to maximize beamforming gain while effectively minimizing interference.

To enhance clustered-AP network performance, we propose optimizing pilot power allocation to improve users’ SINR during training. The system dynamically adjusts pilot powers to maximize the weighted sum-rate under power constraints, formulated as a WSRM problem solved via quadratic transform. This ensures consistent, high-quality service, with numerical results showing superior spectral efficiency compared to benchmarks. The key contributions and findings are summarized as follows:

- The proposed scheme enhances uplink CFmMIMO SE by dynamically clustering APs and allocating pilot power. AP clusters are formed using a hierarchical correlation-based method, associating users with APs that offer both strong channel gains and low correlation to ensure reliable connectivity and reduced interference.
- The method allows flexible cluster adjustments without full network reclustering, reducing CSI re-estimation and minimizing network-wide overhead.
- User–AP associations maximize coherent combining gains and reduce interference by selecting APs with strong, low-correlated channels, achieving balanced service quality (though at the cost of higher backhaul demand).
- Scalability is supported by limiting the number of users per AP, preventing overloads due to hardware limits or pilot reuse, and sustaining performance in dense networks.
- Pilot power allocation is optimized to improve SINR during training, formulated as a WSRM problem and solved for consistent, high-quality service.

C. Outline

The remainder of the paper is organized as follows. Section II describes the system model. Section III introduces the proposed algorithm for AP selection and pilot power

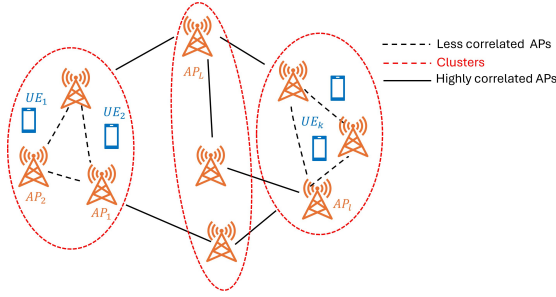


Fig. 1: AP clustering for CFmMIMO system.

allocation, aimed at optimizing AP clustering and improving SE. This section also provides a summary of the algorithms and an analysis of their computational complexity. Section IV presents simulation results, demonstrating the advantages of the proposed approach. Finally, Section V concludes the paper.

D. Notations

We represent vectors using bold lowercase letters and matrices using bold uppercase letters. $\mathbb{E}\{\cdot\}$ stands for the statistical expectation of random variables, and a circular symmetric complex Gaussian matrix with covariance \mathbf{Z} is denoted by $\mathcal{CN}(0, \mathbf{Z})$. The diagonal matrix operator is denoted by $\text{diag}(\cdot)$. The sets of complex and real numbers are represented by \mathbb{C} and \mathbb{R} , respectively. The notations $(\cdot)^T$, $(\cdot)^*$, $(\cdot)^{-1}$, and $(\cdot)^H$ denote the transpose, conjugate, inverse, and conjugate transpose (Hermitian), respectively. The Euclidean norm and absolute value are written as $\|\cdot\|$ and $|\cdot|$, respectively. Superscripts p and d are used to indicate variables or parameters related to pilot and data transmission, respectively. The notation $(\cdot)^\downarrow$ denotes descending order, and \mathbf{I} represents the identity matrix.

II. SYSTEM MODEL

We consider a scalable CFmMIMO system as shown in Fig. 1 with L randomly distributed APs that serve U single-antenna UEs; a reasonable assumption should be $U \ll L$. All APs are equipped with M antennas and connected to a CPU via fronthaul links. The system operates in time-division duplex (TDD) mode, and we assume that all APs and users are perfectly synchronized. For each user u , a subset of APs denoted by \mathcal{A}_u is selected to provide service as described in III-A. We consider a system that operates in a block-fading channel, where the time and frequency plane is divided into coherence blocks, τ_c , in which τ and $\tau_c - \tau$ denote the uplink pilot and data transmission durations (in symbols), respectively. The channel between the l^{th} AP and the u^{th} user is denoted by the channel $\mathbf{h}_{lu} \in \mathbb{C}^{M \times 1}$. In each block, an independent realization from a correlated Rayleigh fading distribution is drawn as $\mathbf{h}_{lu} \sim \mathcal{CN}(0, \mathbf{B}_{lu})$ where $\beta_{lu} = \text{tr}(\mathbf{B}_{lu})/M$ is the large-scale fading that describes geometric pathloss and shadowing, and $\mathbf{B}_{lu} = \mathbb{E}\{\hat{\mathbf{h}}_{lu} \hat{\mathbf{h}}_{lu}^H\}$.

A. Uplink Training and Channel Estimation

We consider τ mutually orthogonal pilot sequences $\{\phi_1, \dots, \phi_\tau\}$ of length τ , such that $\|\phi_t\|^2 = \tau$. These pilots

are assigned to UEs in a deterministic but otherwise arbitrary manner. Since in practical networks $U > \tau$, multiple UEs must share the same pilot. The pilot index assigned to UE u is denoted by $t_u \in \{1, \dots, \tau\}$, and we define $\mathcal{P}_u \subseteq \{1, \dots, U\}$ as the set of UEs reusing pilot t_u , including UE u .

During the uplink training phase, the received pilot signal at AP l , denoted by $\mathbf{Y}_l \in \mathbb{C}^{M \times \tau}$, is given by

$$\mathbf{Y}_l = \sum_{i=1}^U \sqrt{p_i^p} \mathbf{h}_{li} \phi_{t_i}^T + \mathbf{N}_l, \quad (1)$$

where p_i^p is the transmit power of UE i , and $\mathbf{N}_l \in \mathbb{C}^{M \times \tau}$ is the receiver noise matrix with i.i.d. entries distributed as $\mathcal{N}_{\mathbb{C}}(0, \sigma^2)$. To estimate the channel of UE i , AP l correlates \mathbf{Y}_l with the normalized pilot $\phi_{t_u}/\sqrt{\tau}$, yielding

$$\mathbf{r}_l^p = \frac{1}{\sqrt{\tau}} \mathbf{Y}_l \phi_{t_u}^* = \sum_{i \in \mathcal{P}_u} \sqrt{p_i^p \tau} \mathbf{h}_{li} + \mathbf{n}_l^p, \quad (2)$$

where $\mathbf{n}_l^p = \mathbf{N}_l \phi_{t_u}^*/\sqrt{\tau} \sim \mathcal{N}_{\mathbb{C}}(\mathbf{0}, \sigma^2 \mathbf{I}_M)$. Using standard MMSE estimation theory [56], the channel estimate of \mathbf{h}_{lu} is

$$\hat{\mathbf{h}}_{lu} = \sqrt{p_u^p \tau} \mathbf{B}_{lu} \Psi_{l_{t_u}}^{-1} \mathbf{r}_l^p, \quad (3)$$

where $\Psi_{l_{t_u}} = \mathbb{E}\{\mathbf{r}_l^p (\mathbf{r}_l^p)^H\} = \sum_{i \in \mathcal{P}_u} \tau p_i^p \mathbf{B}_{li} + \sigma^2 \mathbf{I}_M$. The estimate and error are independent Gaussian vectors with

$$\hat{\mathbf{h}}_{lu} \sim \mathcal{N}_{\mathbb{C}}(\mathbf{0}, p_u^p \tau \mathbf{B}_{lu} \Psi_{l_{t_u}}^{-1} \mathbf{B}_{lu}). \quad (4)$$

Since multiple UEs reuse the same pilot, the correlated term in (2) introduces interference, leading to the well-known *pilot contamination* effect that degrades channel estimation accuracy, similar to conventional cellular mMIMO systems.

To ensure system scalability, we define a matrix $\mathbf{A} \in \mathbb{R}^{L \times U}$ that specifies the AP-UE associations, where $\mathbf{A}_{lu} = 1$ indicates that user u is served by AP l , and $\mathbf{A}_{lu} = 0$ otherwise. For clarity we define $\mathcal{A}_u = \{l : \mathbf{A}_{lu} = 1, l \in \{1, \dots, L\}\}$ as the subset of APs assigned to serve user u .

B. Uplink Data Transmission and Achievable SE

During the uplink data transmission, all UEs send their data to the APs using the same time-frequency resource. The received signal, $\mathbf{r}_l^d \in \mathbb{C}^{M \times 1}$, at the l^{th} AP is given by

$$\mathbf{r}_l^d = \sum_{i=1}^U \sqrt{p_i^d} \mathbf{h}_{li} s_i + \mathbf{n}_l^d, \quad (5)$$

where p_i^d is the transmit data power of user i , s_i with $\mathbb{E}\{|s_i|^2\} = 1$, is the data symbol transmitted by u^{th} user, and $\mathbf{n}_l^d \in \mathcal{CN}(0, \sigma^2 \mathbf{I}_M)$ is the additive white Gaussian noise. For signal detection in the first stage, the l^{th} AP utilizes the maximum ratio combining technique in which the received signal, \mathbf{r}_l^d is multiplied by the Hermitian transpose of the channel estimate, $\hat{\mathbf{h}}_{lu}^H$ and transmits $\hat{\mathbf{h}}_{lu}^H \mathbf{r}_l^d$ to the CPU through the backhaul link for all users. Then, for each user, u , the

$$\begin{aligned}
\text{SINR}_u &= \frac{p_u^d \left| \sum_{l \in \mathcal{A}_u} \mathbb{E} \left\{ \hat{\mathbf{h}}_{lu}^H \mathbf{h}_{lu} \right\} \right|^2}{\sum_{i=1}^U p_i^d \mathbb{E} \left\{ \left| \sum_{l \in \mathcal{A}_u} \hat{\mathbf{h}}_{lu}^H \mathbf{h}_{li} \right|^2 \right\} - p_u^d \left| \sum_{l \in \mathcal{A}_u} \mathbb{E} \left\{ \hat{\mathbf{h}}_{lu}^H \mathbf{h}_{lu} \right\} \right|^2 + \sigma^2 \sum_{l \in \mathcal{A}_u} \mathbb{E} \left\{ \left\| \hat{\mathbf{h}}_{lu} \right\|^2 \right\}} \\
&= \frac{p_u^d p_u^p \tau \sum_{l \in \mathcal{A}_u} \text{tr}(\mathbf{B}_{lu} \Psi_{l_{tu}}^{-1} \mathbf{B}_{lu})}{\sum_{i=1}^U \sum_{l \in \mathcal{A}_u} \frac{p_i^d \text{tr}(\mathbf{B}_{li} \mathbf{B}_{lu} \Psi_{l_{tu}}^{-1} \mathbf{B}_{lu})}{\text{tr}(\mathbf{B}_{lu} \Psi_{l_{tu}}^{-1} \mathbf{B}_{lu})} + \sum_{\substack{i \in \mathcal{P}_u \\ i \neq u}} \sum_{l \in \mathcal{A}_u} \frac{p_i^p p_u^d \tau \left| \text{tr}(\mathbf{B}_{li} \Psi_{l_{tu}}^{-1} \mathbf{B}_{lu}) \right|^2}{\text{tr}(\mathbf{B}_{lu} \Psi_{l_{tu}}^{-1} \mathbf{B}_{lu})} + \sigma^2}
\end{aligned} \tag{11}$$

received products are combined as

$$\begin{aligned}
r_u &= \sum_{l \in \mathcal{A}_u} \hat{\mathbf{h}}_{lu}^H \mathbf{r}_l^d \\
&= \sum_{l \in \mathcal{A}_u} \left(\hat{\mathbf{h}}_{lu}^H \mathbf{h}_{lu} s_u + \sum_{i=1, i \neq u}^U \hat{\mathbf{h}}_{lu}^H \mathbf{h}_{li} s_i + \hat{\mathbf{h}}_{lu}^H \mathbf{n}_l^d \right). \tag{6}
\end{aligned}$$

Since the CPU does not have the knowledge of the channel estimates, we apply the use-and-then-forget technique [57] to obtain the achievable SE as follows

$$\text{SE}_u = \left(1 - \frac{\tau}{\tau_c}\right) \log_2(1 + \text{SINR}_u), \tag{7}$$

where SINR_u is given at the top of the this page [56] and

$$\mathbb{E} \left\{ \hat{\mathbf{h}}_{lu}^H \mathbf{h}_{lu} \right\} = p_u^p \tau \sum_{l \in \mathcal{A}_u} \text{tr}(\mathbf{B}_{lu} \Psi_{l_{tu}}^{-1} \mathbf{B}_{lu}). \tag{8}$$

$$\mathbb{E} \left\{ \left\| \hat{\mathbf{h}}_{lu} \right\|^2 \right\} = p_u^p \tau \sum_{l \in \mathcal{A}_u} \text{tr}(\mathbf{B}_{lu} \Psi_{l_{tu}}^{-1} \mathbf{B}_{lu}). \tag{9}$$

and

$$\begin{aligned}
\mathbb{E} \left\{ \left| \hat{\mathbf{h}}_{lu}^H \mathbf{h}_{li} \right|^2 \right\} &= p_u^p \tau \sum_{l \in \mathcal{A}_u} \text{tr}(\mathbf{B}_{li} \mathbf{B}_{lu} \Psi_{l_{tu}}^{-1} \mathbf{B}_{lu}) \\
&+ \begin{cases} p_u^p p_i^p \tau^2 \left| \sum_{l \in \mathcal{A}_u} \text{tr}(\mathbf{B}_{li} \Psi_{l_{tu}}^{-1} \mathbf{B}_{lu}) \right|^2 & i \in \mathcal{P}_u \\ 0 & i \notin \mathcal{P}_u \end{cases} \tag{10}
\end{aligned}$$

III. PROPOSED AP SELECTION AND PILOT POWER ALLOCATION

In this section, we present a novel, efficient, and scalable dynamic AP clustering method based on channel correlation, designed to ensure that low-mutually correlated APs serve users with the strongest channel conditions. In addition, we propose a pilot power allocation strategy to enhance each user's SINR during the training phase. The proposed approaches address the weighted sum-rate maximization (WSRM) problem between APs and users.

A. Access Points Clustering

AP selection based on the channel gain is an efficient method in that it reduces complexity, backhaul load, and interference by choosing the APs with the strongest large-scale fading for each user. However, this approach also comes with certain drawbacks. One key limitation is determining the optimal number of APs to select for each user; choosing

too few APs may degrade performance due to insufficient diversity or coverage, while selecting too many can negate the benefits of reduced complexity. Moreover, the selection based purely on channel gain does not consider AP correlation or spatial distribution, which may lead to suboptimal AP clusters and potential interference. On the other hand, to make a CFmMIMO system scalable, the system must adopt an association scheme that limits the maximum number of UEs that can associate with one AP.

To address these challenges, we propose a dynamic clustering approach that groups APs based on the correlation of their channel responses for each user. This strategy ensures that the APs serving a given user exhibit similar channel characteristics, enabling optimization of the user's signal reception. Furthermore, we introduce an adaptive AP-user association scheme designed to enhance scalability as the network grows. The overall procedure is organized into four key stages:

Stage 1: Channel Correlation & AP Clustering

In the proposed clustering formation, we aim to group a subset of the low-mutually correlated APs that provide similar channel conditions to the u^{th} user dynamically. In this regard, the collective channel from all users to l^{th} AP is defined as $\hat{\mathbf{h}}_l = [\hat{\mathbf{h}}_{l1}^T, \hat{\mathbf{h}}_{l2}^T, \dots, \hat{\mathbf{h}}_{lU}^T]^T \in \mathbb{C}^{MU}$. Since we want to find the APs with the lowest correlation and similar channel characteristics that serve the u^{th} user, the correlation coefficient between the channels of two APs, such as l and k , can be expressed as:

$$\rho_{lk} = \frac{\hat{\mathbf{h}}_l^H \hat{\mathbf{h}}_k}{\|\hat{\mathbf{h}}_l\| \|\hat{\mathbf{h}}_k\|}, \quad \forall l, k \in \{1, 2, \dots, L\} \tag{12}$$

This evaluates the correlation between the channel vectors of different APs, ensuring that APs with low mutual correlation are grouped into the same cluster. To this end, we utilize an algorithm that recursively merges or splits APs into nested clusters based on a measure of similarity, ultimately forming a tree-like structure.

We start by defining a distance matrix $\mathbf{D} \in \mathbb{R}^{L \times L}$ and its entries given by $D_{lk} = 1 - \rho_{lk}$. Note that the distance matrix does not represent the physical distances between pairs of APs. Instead, it quantifies the difference in their correlation values, providing a measure of similarity between the APs based on their channel characteristics. Each entry in the matrix corresponds to the computed "distance" in terms of correlation rather than geographic separation. After that, we utilize tree-like clustering to group APs based on their channel correlation. The clustering is based on the correlation coefficients ρ_{lk} and the linkage function, which defines how

to measure the distance between sets of data points. In this clustering, the process starts with each AP as an individual cluster as $\mathcal{C}^{(1)} = \{\{AP_1\}, \{AP_2\}, \dots, \{AP_L\}\}$, which is the initial clustering. Then, the inter-cluster distance $D(C_i, C_j)$ (i.e. $C_i = \{AP_i\}$, $C_j = \{AP_j\}$, $i \neq j$, $\forall i, j \in L$) between any two clusters using the linkage criterion is computed as

$$D(C_i, C_j) = \frac{1}{|C_i||C_j|} \sum_{l \in C_i} \sum_{k \in C_j} D(l, k), \quad (13)$$

where C_i and C_j are the i -th and j -th current clusters ($j \neq i$). Then, the pair of clusters (C_i, C_j) with minimum $D(C_i, C_j)$ is computed as $(i^*, j^*) = \arg \min_{i \neq j} D(C_i, C_j)$. After that, the closest clusters are iteratively merged based on some similarity (or distance) measure as

$$\mathcal{C}^{(n+1)} = \left(\mathcal{C}^{(n)} \setminus \{C_{i^*}, C_{j^*}\} \right) \cup \{C_{i^*}, C_{j^*}\}, \quad (14)$$

where n is the internal iteration of the linkage function. The clustering process continues iteratively until a predefined stopping condition is satisfied. Specifically, the merging of clusters is terminated when the inter-cluster distance exceeds a specified threshold κ . Mathematically, let $D(C_i, C_j)$ denote the distance between clusters C_i and C_j , according to the chosen linkage criterion. The process halts when $\min_{i \neq j} D(C_i, C_j) > \kappa$. At this point, the current partition $\mathcal{C} = \{C_1, C_2, \dots, C_S\}$ defines the final set of clusters, where S is the total number of clusters.

Stage 2: AP-user Association

Once the clusters are formed, AP selection proceeds as follows. For each user, the large-scale fading coefficients from all APs are sorted in descending order to identify the AP with the strongest channel gain. The algorithm then scans through the set of clusters to find the one that contains the strongest AP, \mathcal{I}_u . Once identified, the entire cluster containing the strongest AP is selected to serve the user. This ensures that the selected APs are not only strong individually but also form a spatially low-coherent group with respect to the user.

Note: If the strongest AP appears in more than one cluster (e.g., due to overlapping clusters from multiple users), a cluster resolution strategy is applied. In this case, we prioritize the cluster that maximizes the total sum of large-scale fading coefficients for the user. This helps avoid ambiguous AP assignments and ensures fair and interference-aware clustering. This approach provides a balanced trade-off: it retains the strongest APs for each user while forming clusters that promote coherent signal transmission and efficient interference management.

Stage 3: Scalability Constraint

At this stage, the algorithm incorporates a load-balancing mechanism to prevent any AP from being overloaded with user associations. Each AP is allowed to serve at most τ users simultaneously. Before assigning a candidate cluster C_i to a user u , the algorithm checks the current load N_l of every AP l within that cluster. The assignment is accepted only if all APs in C_i satisfy the condition $N_l < \tau$. Once the assignment is confirmed, the cluster C_i is added to the user's serving set \mathcal{A}_u , and the counters N_l for the corresponding APs are incremented. This stage guarantees that the association

process remains scalable with respect to network size and user density while keeping pilot contamination and interference under control.

Stage 4: Overflow Handling

When the candidate cluster C_i for user u contains one or more APs that have already reached their service limit τ , the algorithm activates an overflow management mechanism to maintain balanced resource allocation. Two complementary strategies are employed: *i. Partial Assignment:* The algorithm first filters out the saturated APs from C_i and retains only the subset of APs with available capacity, and this subset serves the user. *ii. Cluster Reassignment:* If all APs in C_i are saturated and no valid subset remains, the algorithm searches for an alternative cluster $C_{i^{\text{alt}}}$ with sufficient remaining capacity. The selection criterion is to maximize the aggregate channel gain $\sum_{l \in C_{i^{\text{alt}}}} \beta_{lu}$ while respecting the constraint $N_l < \tau$. The user is then associated with this alternative cluster. This stage ensures fair distribution of network resources, prevents excessive load concentration on a few APs, and maintains service quality even in dense deployment scenarios. The full procedure is outlined in Algorithm 1.

B. Pilot power allocation

The CFmMIMO system operates in TDD mode, with channels estimated at each AP based on user pilot signals during the training phase. However, due to the non-orthogonality of pilot sequences, the channel estimates for a given user are corrupted by interference from pilots sent by other users, a phenomenon known as pilot contamination [2]. This issue is particularly pronounced where the goal is to simultaneously serve a large number of users within the same time-frequency resources. As a result, mitigating pilot contamination is critical. To tackle pilot contamination, recent studies have introduced various algorithms aimed at mitigating its effects, especially in densely populated multi-user settings, to improve communication quality by reducing interference from pilot reuse [58], [59]. However, this work assumes a scenario with substantial pilot contamination resulting from random pilot assignment. This assumption enables the evaluation of the proposed method's performance under challenging, worst-case conditions. Thus, we propose a solution optimizing pilot power allocations to maximize each user's SINR during the training phase.

1) Weighted sum-rate maximization problem: Given the objective of providing a better quality of service to all users, we formulate this as a WSRM problem [60]. The system dynamically adjusts pilot powers to maximize the weighted sum of users' data rates subject to power constraints as follows

$$P_1 : \max_{\mathbf{p}_u^p} \sum_{u=1}^U w_u \text{SE}_u(\mathbf{p}_u^p, \mathbf{p}_u^d) \quad \text{s.t.} \quad \epsilon \leq p_u^p \leq P_{\max} \quad \forall u, \quad (15)$$

where w_u is a weight associated with the u^{th} user (representing user priority) and P_{\max} denotes the maximum transmit budget available for each user while $\epsilon > 0$ is small value. Also, we have assumed that the data power, \mathbf{p}_u^d , is fixed and distributed between all users equally. It is clear from the optimization

Algorithm 1: Proposed scalable method

```

1 Input:  $\hat{\mathbf{h}}_{lu}, u = 1, \dots, U, \kappa, \tau, \mathcal{C}$ : clustered APs,  $\mathcal{A}_u$ : set
   of APs serving user  $u$ ;
2 Initialization:  $\mathcal{A}_1 = \dots = \mathcal{A}_U = \emptyset; N_l = 0, \forall l$ 
3 for channel realization do
4   Define  $\hat{\mathbf{h}}_l = [\hat{\mathbf{h}}_{l1}^T, \dots, \hat{\mathbf{h}}_{lU}^T]^T \in \mathbb{C}^{MU}$ ;
5    $\rho_{lk} = \frac{\hat{\mathbf{h}}_l \hat{\mathbf{h}}_k^H}{\|\hat{\mathbf{h}}_l\| \|\hat{\mathbf{h}}_k\|}, \mathbf{D} = \mathbf{I} - \rho_{lk}$ 
6   Initialize  $\mathcal{C}^{(1)} = \{\{AP_1\}, \dots, \{AP_L\}\}$ ;
7   while  $\min_{i \neq j} D(C_i, C_j) > \kappa$  do
8      $D(C_i, C_j) = \frac{1}{|C_i| |C_j|} \sum_{l \in C_i} \sum_{k \in C_j} D(l, k)$ ;
9      $(i^*, j^*) = \arg \min_{i \neq j} D(C_i, C_j)$ ;
10     $\mathcal{C}^{(n+1)} = (\mathcal{C}^{(n)} \setminus \{C_{i^*}, C_{j^*}\}) \cup \{C_{i^*} \cup C_{j^*}\}$ ;
11  end
12   $\mathcal{C} = \{C_1, \dots, C_s, \dots, C_S\}$ ;
13  for  $u = 1 : U$  do
14     $\text{APs}_u \leftarrow \text{argsort}_l(\hat{\mathbf{h}}_{lu})^\dagger$ ;
15     $l^* \leftarrow \text{APs}_u(1)$ ;
16     $\mathcal{I}_u \leftarrow \{s \mid l^* \in C_s\}$ ;
17    if  $|\mathcal{I}_u| = 1$  then
18       $i \leftarrow \mathcal{I}_u(1)$ ;
19    else
20       $i \leftarrow \arg \max_{s \in \mathcal{I}_u} \sum_{l \in C_s} \hat{\mathbf{h}}_{lu}$ ; // highest total
21      gain cluster
22    if  $N_l < \tau \forall l \in C_i$  then
23       $\mathcal{A}_u \leftarrow C_i$ ;
24      for  $l \in C_i$  do
25         $N_l \leftarrow N_l + 1$ 
26      end
27    else
28      // partial assignment
29       $C_{\text{valid}} \leftarrow \{l \in C_i \mid N_l < \tau\}$ ;
30      if  $C_{\text{valid}} \neq \emptyset$  then
31         $\mathcal{A}_u \leftarrow l \in C_{\text{valid}}$ ;
32        for  $l \in \mathcal{A}_u$  do
33           $N_l \leftarrow N_l + 1$ 
34        end
35      else
36        // reassignment
37        for  $s = 1 : S$  do
38           $\text{gain}(s) = \sum_{l \in C_s, N_l < \tau} \hat{\mathbf{h}}_{lu}$ ;
39        end
40         $i^{\text{alt}} = \arg \max_s \text{gain}(s)$  // alternative
41         $\mathcal{A}_u \leftarrow \{l \in C_{i^{\text{alt}}} \mid N_l < \tau\}$ ;
42        for  $l \in \mathcal{A}_u$  do
43           $N_l \leftarrow N_l + 1$ 
44        end
45      end
46    end
47  end
Output:  $\mathcal{A}_u$  for all  $u$ 

```

problem in (15) that the SE for each user u depends on their SINR, which is a function of the power allocation as follows

$$P_1: \max_{\mathbf{p}_u^p} \sum_{u=1}^U w_u \log_2(1 + \text{SINR}_u(\mathbf{p}_u^p, \mathbf{p}_u^d)),$$

$$\text{s.t. } \epsilon \leq p_u^p \leq P_{\max} \quad \forall u, \quad (16)$$

Although the problem P_1 is an NP-hard problem [61], it can be solved using a quadratic transform for multiple-ratio fractional programming [62]. In this problem, it is seen that the power control problem is not explicitly in a ratio form, but the key components of the objective function, namely, the SINR terms, exhibit a fractional structure. Since each SINR expression appears within a logarithmic function, which is concave and non-decreasing, we can solve it using the following corollary. *Corollary 1:* Given a sequence of non-decreasing functions $f_m(\cdot)$ and a sequence of ratios A_m/B_m for $m = 1, \dots, M$, the sum-of-functions-of-ratio problem

$$\max_{\mathbf{x}} \sum_{m=1}^M f_m\left(\frac{A_m(\mathbf{x})}{B_m(\mathbf{x})}\right) \quad \text{s.t. } \mathbf{x} \in \mathcal{X} \quad (17)$$

is equivalent to

$$\max_{\mathbf{x}, \mathbf{y}} \sum_{m=1}^M f_m\left(2y_m \sqrt{A_m(\mathbf{x})} - y_m^2 B_m(\mathbf{x})\right) \quad (18a)$$

$$\text{s.t. } \mathbf{x} \in \mathcal{X}, y_m \in \mathbb{R}, m = 1, \dots, M \quad (18b)$$

To verify Corollary 1, problem (17) is reformulated as

$$\max_{\mathbf{x}, \mathbf{r}} \sum_{m=1}^M f_m(r_m) \quad \text{s.t. } \mathbf{x} \in \mathcal{X}, r_m = \frac{A_m(\mathbf{x})}{B_m(\mathbf{x})} \quad (19)$$

Applying the quadratic transform introduced in [62], each ratio term r_m can be equivalently expressed as

$$r_m = \max_{y_m} \left(2y_m \sqrt{A_m(\mathbf{x})} - y_m^2 B_m(\mathbf{x})\right), \quad (20)$$

where y_m is the auxiliary available. Since $f_m(\cdot)$ is nondecreasing, the problem becomes

$$\max_{\mathbf{x}} \sum_{m=1}^M f_m\left(\max_{y_m} (2y_m \sqrt{A_m(\mathbf{x})} - y_m^2 B_m(\mathbf{x}))\right). \quad (21)$$

Finally, by combining the outer maximization over \mathbf{x} and the inner maximization over \mathbf{y} , we obtain the equivalent formulation given in (18a).

The optimization problem in (18) can be solved using an iterative approach by applying the quadratic transform, which alternates between optimizing the primal variable \mathbf{x} and updating y_m in closed form as follows:

When we hold \mathbf{x} fixed, the optimal y_m that maximizes the objective function can be obtained by taking the first-order derivative of (21) and setting it to zero

$$y_m^* = \frac{\sqrt{A_m(\mathbf{x})}}{B_m(\mathbf{x})}, \forall m = 1, \dots, M. \quad (22)$$

When y_m is fixed, due to the concavity of each $A_m(\mathbf{x})$, the convexity of each $B_m(\mathbf{x})$, and the fact that the square-root

Algorithm 2: Iterative Approach for Concave-Convex fractional problem in (17)

- 1 **Step 0:** Initialize \mathbf{x} to a feasible value ;
 - 2 **Step 1** Reformulate the problem by the quadratic transform, i.e., replace each A_m/B_m with $2y_m\sqrt{A_m} - y_m^2B_m$;
 - 3 **repeat**
 - 4 **Step 2:** Update \mathbf{y} by (22)
 - 5 **Step 3:** Update \mathbf{x} by solving the reformulated convex optimization problem (18a), over \mathbf{x} for fixed \mathbf{y}
 - 6 **until** convergence;
-

function is concave and increasing, the quadratic transform

$$g(\mathbf{x}, y_m) = 2y_m\sqrt{A_m(\mathbf{x})} - y_m^2B_m(\mathbf{x}), \quad (23)$$

is concave in \mathbf{x} . Further, if $f_m(\cdot)$ is assumed to be concave and nondecreasing, then we also have that $f_m(g(\mathbf{x}, y_m))$ is concave in \mathbf{x} . Therefore, the quadratic transformed problem (18a) is a concave maximization problem over \mathbf{x} . The optimal \mathbf{x} can thus be efficiently obtained through numerical convex optimization. The entire approach is summarized in Algorithm 2 [62].

It can be shown by the below theorem that Algorithm 2 will achieve a stationary point of concave-convex fractional programming problems.

Theorem 1: For the concave-convex sum-of-functions-of-ratio problem (17), i.e., every $A_m(\mathbf{x})$ is concave and every $B_m(\mathbf{x})$ is convex, and \mathcal{X} is a convex set in standard form, and assuming further that f_m is non-decreasing and concave, then Algorithm 2 consists of a sequence of convex optimization problems that converge to a stationary point of (17) with non-decreasing sum-of-functions-of-ratio value after every iteration.

Proof: The algorithm is essentially a block coordinate ascent algorithm for the reformulated problem (18), which is a convex optimization problem due to the concave-convex form of (17), so it converges to a stationary point $(\mathbf{x}^*, \mathbf{y}^*)$ of (18). Due to the equivalence in the solution and the equivalence in the objective value, the first-order condition on \mathbf{x} for (18) under the optimal \mathbf{y} is the same as for the original problem (17), hence the algorithm also converges to a stationary point of (17). Also, the sum-of-ratio function is nondecreasing after each \mathbf{y} update.

Using this theorem and according to (18), the problem in P_1 can be written as

$$P_2 : \max_{\{p_u^p, y_u\}} \sum_{u=1}^U w_u \left(2y_u \sqrt{A_u(p_u^p)} - y_u^2 B_u(p_{-u}^p) \right) \quad (24a)$$

$$\epsilon \leq p_u^p \leq P_{\max}, \quad u = 1, \dots, U \quad (24b)$$

$$y_i \in \mathbb{R}, \quad (24c)$$

From (11), the terms $A_u(p_u^p)$ and $B_u(p_{-u}^p)$ correspond to the numerator and denominator, respectively. Problem 2 (P_2) is solved through an iterative procedure, as outlined in Algorithm 3.

Fig. 2 depicts the convergence performance of the proposed power allocation scheme for different pilot sequences with $U = 40$ users and $L = 100$ APs.

Algorithm 3: Power Control Approach

Input: Initial pilot powers $\{p_u^p(0)\} \in [\epsilon, P_{\max}]$, weights $\{w_u\}$, tolerance δ , max iterations N_{\max}

Output: Optimized pilot powers $\{p_u^{p*}\}$

- 1 **Initialize:** $p_u^p(0) \leftarrow P_{\max}/2, \forall u$, iteration $n \leftarrow 0$;
- 2 **repeat**

// Step 1: Update auxiliary variables y_u

- 3 **for** $u = 1 : U$ **do**
- 4 $y_u \leftarrow \frac{\sqrt{A_u(p_u^p)}}{B_u(p_{-u}^p)}$;
- 5 **end**

// Step 2: Update pilot powers $\{p_u^p\}$

- 6 Solve the following problem via CVX [63]:

$$\begin{aligned} \max_{\{p_u^p\}} \quad & \sum_{u=1}^U w_u \left(2y_u \sqrt{A_u(p_u^p)} - y_u^2 B_u(p_{-u}^p) \right) \\ \text{s.t.} \quad & \epsilon \leq p_u^p \leq P_{\max}, \quad \forall u. \end{aligned}$$

- 7 **Update:** $\mathbf{p}^p(n+1) \leftarrow \{p_u^p\}$;

- 8 $n \leftarrow n + 1$;

- 9 **until** $\frac{\|\mathbf{p}^p(n) - \mathbf{p}^p(n-1)\|}{\|\mathbf{p}^p(n-1)\|} < \delta$;

- 10 **return** $\{p_u^{p*}\} \leftarrow \mathbf{p}^p(n)$
-

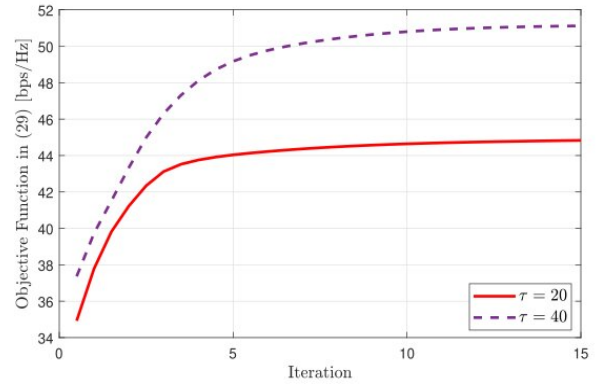


Fig. 2: Convergence of the iterative algorithm for $L = 100, M = 1, U = 40$.

C. Data Power Control

One important aspect of CFmMIMO systems is their capability to provide consistently uniform service across users. We focus on the optimization problem of max-min fairness, which entails using the pilot power coefficients calculated in Algorithm 1 ($\hat{\mathbf{p}}_u^p$) and optimizing the data power control coefficient to maximize the minimum user rates. We denote the data power coefficient vector as $\mathbf{p}_u^d = [p_1^d, p_2^d, \dots, p_U^d]$, then rewrite the uplink SE of u^{th} user as

$$\text{SE}_u(\hat{\mathbf{p}}_u^p, \mathbf{p}_u^d) = \left(1 - \frac{\tau}{\tau_c}\right) \log_2 \left(1 + \text{SINR}_u(\hat{\mathbf{p}}_u^p, \mathbf{p}_u^d)\right), \quad (25)$$

and the optimization problem is formulated as:

$$P_3 : \max_{\{p_u^d\}} \min_{u=1, \dots, U} \text{SE}_u(\hat{\mathbf{p}}_u^p, \mathbf{p}_u^d) \quad \text{s.t.} \quad 0 \leq p_u^d \leq 1, \quad \forall u \in U \quad (26)$$

where $\text{SE}_u(\hat{\mathbf{p}}_u^p, \mathbf{p}_u^d)$ is defined in (25). The optimal data power, p_u^d can be determined by solving the following max-min

problem:

$$P_4 : \max_{\{p_u^d\}} \min_{u=1, \dots, U} \text{SINR}_u(\hat{\mathbf{p}}_u^p, \mathbf{p}_u^d) \quad \text{s.t.} \quad 0 \leq p_u^d \leq 1, \quad \forall u \in U \quad (27)$$

Without loss of generality, problem P_3 can be rewritten by introducing a new slack variable as

$$P_4 : \max_{\{p_k^d\}, t} t \quad \text{s.t.} \quad t \leq \text{SINR}_u(\hat{\mathbf{p}}_u^p, \mathbf{p}_u^d), \quad (28a)$$

$$0 \leq p_u^d \leq 1, \quad \forall u \in U, \quad (28b)$$

To tackle this optimization problem and explicitly expand the SINR_u expression in (11), we focus on the special case of spatially uncorrelated fading, i.e., $\mathbf{B}_{lu} = \beta_{lu} \mathbf{I}_M$. Under this assumption, (11) simplifies to

$$\frac{M\tau p_u^d p_u^p \sum_{l \in \mathcal{A}_u} \beta_{lu}^2 \psi_l^{-1}}{\sum_{l \in \mathcal{A}_u} (M\tau \sum_{\substack{i \in \mathcal{P}_u \\ i \neq u}} p_i^d p_i^p \beta_{li}^2 \psi_l^{-1} + \sum_{i=1}^U p_i^d \beta_{li}) + \sigma^2} \quad (29)$$

where $\psi_l = \tau \sum_{i \in \mathcal{P}_u} p_i^p \beta_{li} + \sigma^2$.

Proposition 2: The problem P_4 can be reformulated as a geometric program (GP) [64].

Proof: Based on the standard form of a geometric progression in [65] we can reformulate the SINR constraint in (28a) as

$$\frac{\sum_{l \in \mathcal{A}_u} (M\tau \sum_{\substack{i \in \mathcal{P}_u \\ i \neq u}} p_i^d p_i^p \beta_{li}^2 \psi_l^{-1} + \sum_{i=1}^U p_i^d \beta_{li} + \sigma^2)}{M\tau p_u^d p_u^p \sum_{l \in \mathcal{A}_u} \beta_{lu}^2 \psi_l^{-1}} < \frac{1}{t} \quad (30)$$

With a straightforward transformation, the SINR constraint in (28a) can be expressed as the following inequality:

$$\frac{1}{p_u^d} \left(\sum_{\substack{i \in \mathcal{P}_u \\ i \neq u}} e_{ui} p_i^d + \sum_{i=1}^U f_{ui} p_i^d + b_u \right) < \frac{1}{t} \quad (31)$$

where

$$e_{ui} = \frac{\sum_{l \in \mathcal{A}_u} p_i^p \beta_{li}^2}{p_u^p \sum_{l \in \mathcal{A}_u} \beta_{lu}^2}, \quad f_{ui} = \frac{\sum_{l \in \mathcal{A}_u} \beta_{li}}{M\tau p_u^p \sum_{l \in \mathcal{A}_u} \beta_{lu}^2 \psi_l^{-1}} \quad (32)$$

$$b_u = \frac{\sigma^2}{M\tau p_u^p \sum_{l \in \mathcal{A}_u} \beta_{lu}^2 \psi_l^{-1}}$$

The transformation in (31) reveals that the left-hand side is a posynomial function. Consequently, problem P_4 meets the criteria for a standard GP problem, thereby validating the proof of Proposition 2. As stated in Proposition 2, the objective function and constraints of P_4 consist of monomial and posynomial functions with respect to the power allocations p_u^d . This confirms that P_4 is a standard GP, which can be efficiently solved using convex optimization tools.

D. Complexity Analysis of the Proposed Method

The computational complexity of the scalable AP-user association algorithm is mainly determined by three components. First, computing the AP-AP correlation matrix requires evaluating the correlation coefficient for all $L(L-1)/2$ AP pairs, each involving an inner product over U users, leading to a

complexity of $\mathcal{O}(L^2U)$. Second, the hierarchical clustering stage, implemented via agglomerative merging, requires identifying and merging the closest cluster pair at each iteration, which in the naive implementation leads to $\mathcal{O}(L^2)$ operations in the worst case. Third, ranking the APs for each user based on channel gains involves sorting L values per user, yielding $\mathcal{O}(UL \log L)$ complexity. Final overall complexity is $\mathcal{O}(L^2 + L^2U + UL \log L)$, which simplifies to $\mathcal{O}(L^2)$.

The computational complexity of the proposed power control algorithm (Algorithm 3) is primarily determined by the iterative nature of the method and the convex optimization solved at each iteration. In each iteration, the auxiliary variables y_u for all U users are updated with a complexity on the order of $\mathcal{O}(U^2)$, assuming the computation of functions $A_u(\cdot)$ and $B_u(\cdot)$ involves summations over all users. The dominant computational cost arises from solving the convex optimization problem via CVX, which involves U variables and has a worst-case complexity approximately $\mathcal{O}(U^3)$ when using interior-point methods. Considering that the algorithm runs for at most N_{\max} iterations until convergence, the overall complexity can be expressed as $\mathcal{O}(N_{\max}U^3)$. This cubic complexity with respect to the number of users reflects the computational demand of the pilot power optimization step in CFmMIMO systems, while the optimization solver for the data power problem P_3 in (26) incurs complexity of $\mathcal{O}(U^{3.5})$. The computational complexity of the compared approaches is summarized in Table I.

TABLE I Complexity Comparison of the Benchmarks.

Schemes	Computational complexity
DAPPA	$\mathcal{O}(U^{3.5} + \mathcal{A}_u ^2)$
GB [66]	$\mathcal{O}(U^3 L^2 M^2 + U^2 L M \tau + U M \log_2 M)$
DCC [10]	$\mathcal{O}((M\tau + M^2) \mathcal{A}_u ^2 U)$
NEEPC [44]	$\mathcal{O}(\mathcal{I}_{\text{outer}}(\max((27U^{3.5}), 9(M+5)U^2)))$
DLPC [43]	$\mathcal{O}(L^3 + L^2 U M \log_2 L)$
SAT [46]	$\mathcal{O}(\mathcal{I}_{\text{outer}} \cdot \mathcal{I}_{\text{inner}} \cdot U^4)$

where $\mathcal{I}_{\text{outer}}$ and $\mathcal{I}_{\text{inner}}$ are the outer and inner iterations of the methods in [44] and [46].

IV. NUMERICAL RESULTS

A. Propagation Model

This section presents numerical results to assess the performance of the proposed approach under various CFmMIMO scenarios. While many recent studies on uplink maximum ratio combining have adopted the propagation model from [2], it is important to recognize that this model is derived from the COST-Hata framework in [67], originally designed for macro-cell environments. Specifically, it assumes that APs are deployed at heights of at least 30 meters, and UEs are located at distances exceeding 1 km from the APs. These assumptions significantly differ from the dense, micro-cell-like deployments expected in CFmMIMO systems. Notably, the authors of the COST-Hata model explicitly indicated that it “must not be used for micro-cells” [9]. To ensure a fair and meaningful performance evaluation, we consider both propagation models from [2] and [10], and select the most

appropriate model based on comparative simulation results, as illustrated in Fig. 3.

We consider simulation setups with L APs with M antennas, and U single antenna users. Each coherence block contains $\tau_c = 200$ samples, and the total number of distributed antenna elements across the network is given by LM . Unless otherwise stated, $\tau = 20$ symbols are reserved for uplink pilot transmission, and each user uses its full transmit power 100 mW for pilot signaling. We performed 1000-channel realizations. It is assumed that APs and users are independently and uniformly distributed within an area of 1×1 km², and a wrap-around technique is used to prevent boundary effects and simulate a network with an infinite area. The following three-slope propagation model was used in [2]:

$$\beta_{lu} = \begin{cases} -81.2, & d_{lu} < d_0 \\ -61.2 - 20 \log_{10} \left(\frac{d_{lu}}{1} \right), & d_0 \leq d_{lu} < d_1 \\ -35.7 - 35 \log_{10} \left(\frac{d_{lu}}{1} \right) + F_{lu}, & d_{lu} \geq d_1 \end{cases} \quad (33)$$

where $d_0 = 10$ m, $d_1 = 50$ m and d_{lu} is the horizontal distance between the user u and AP l (i.e., ignoring the height difference). The shadowing term $F_{lu} \sim \mathcal{CN}(0, 8^2)$ only appears when the distance is larger than 50 m and the terms are correlated as

$$\mathbb{E}\{F_{lu}F_{ji}\} = \frac{8^2}{2} \left(2^{-\delta_{ui}/100} + 2^{-\rho_{lj}/100} \right) \quad (34)$$

where δ_{ui} is the distance between UE u and UE i and ρ_{lj} is the distance between AP l and AP j . The maximum user power is 100 mW, the bandwidth is 20 MHz, and the noise power is 92 dBm. The large-scale fading coefficient (channel gain) in [10] is modeled as:

$$\beta_{lu} = -30.5 - 36.7 \log_{10} \left(\frac{d_{lu}}{1} \right) + F_{lu} \quad (35)$$

where d_{lu} is the three-dimensional distance between AP l and the user u . The APs are deployed 10 m above the plane where the users are located, which acts as the minimum distance. This model matches the 3GPP Urban Microcell model in [68]. The shadow fading is $F_{lu} \sim \mathcal{N}(0, 4^2)$ and the terms from an AP to different users are correlated as [68]

$$\mathbb{E}\{F_{lu}F_{ji}\} = \begin{cases} 4^2 2^{-\delta_{ui}/9} & l = j \\ 0 & l \neq j \end{cases} \quad (36)$$

As shown in Fig. 3, due to the limitations of the COST-Hata-based model in [2] for micro-cell scenarios—and in accordance with the recommendation in [9]—this work adopts the propagation model introduced in [10]. This model is better suited for dense and distributed AP deployments in CFmMIMO systems and offers a more realistic assessment of system performance.

B. Simulation Results

In this section, we evaluate the performance of the proposed power allocation and AP selection strategies detailed in Algorithms 1 and 3. The simulation results are organized into three subsections: the first examines the AP selection method using Algorithm 1; the second compares the power allocation

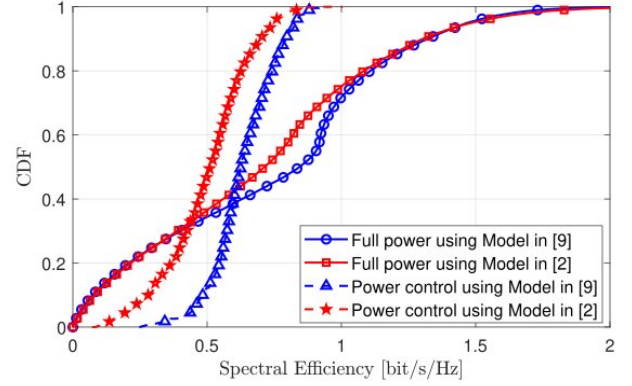


Fig. 3: SE comparison of the proposed method in two propagation models in [2] and [10] for $L = 100$, $M = 1$, $U = 40$, and $\tau = 20$.

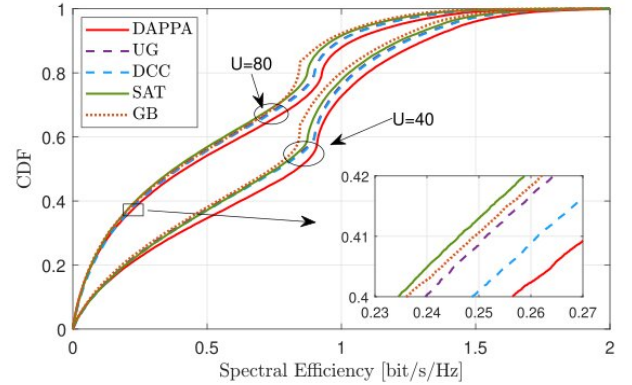


Fig. 4: SE performance for different AP selection schemes with uniform power control with $\tau = 20$, $L = 100$ APs, $M = 1$ antennas, $U = 40$ and $U = 80$ users

strategy from Algorithm 3 against alternatives when all APs are active; and the third evaluates the combined performance of AP selection and power allocation under the proposed scheme.

1) *Results based on the AP selection and the equal power allocation:* In the first part of the simulation, we compare the proposed AP selection method with the scenario where only AP selection is considered, and the power is distributed equally among users. The proposed dynamic access point selection and pilot power allocation (DAPPA) is compared with well-known techniques such as dynamic cooperation clustering (DCC) in [10], user-group based pilot assignment (UG) in [18], graph-based (GB) AP clustering in [66], and successive approximation technique (SAT) in [46]. Fig. 4 depicts the cumulative distribution function (CDF) of the SE for five AP selection schemes under uniform power allocation (It means that, the pilot signals are transmitted by all UEs with full power for all considered schemes), with $\tau = 20$, $L = 100$ APs, $M = 1$ antenna, and two different user counts, $U = 40$ and $U = 80$. For both user scenarios, the proposed method consistently indicates higher SE across most percentiles. In the $U = 40$ case, the proposed scheme offers. The proposed scheme delivers substantial SE improvements for nearly 80%

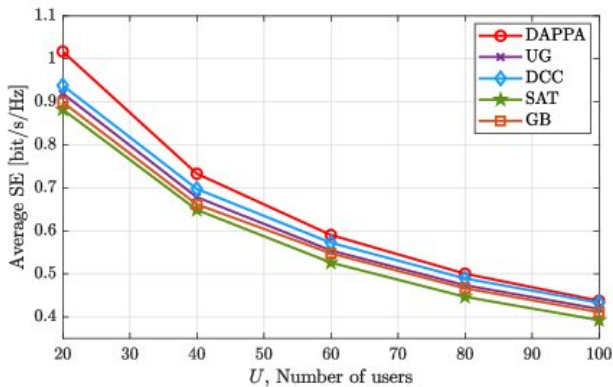


Fig. 5: Impact of increasing user density on the average SE performance of different AP selection schemes with $\tau = 20$, $L = 100$ APs, $M = 1$ antenna, and varying numbers of users.

of the users, outperforming all other approaches. The inset zoom highlights that, at low SE values, the proposed scheme yields marginally higher performance, suggesting better service for far users. For $U = 80$, all schemes exhibit reduced SE due to increased interference and resource contention, yet the proposed method maintains superiority, particularly in the median SE region, where it surpasses the DCC method by a visible margin. UG and DCC remain competitive with each other, while GB slightly outperforms SAT in most ranges. Overall, the results show that the proposed approach given in Algorithm 1 delivers a dynamic clustering approach that groups APs based on the correlation of their channel responses for each user. It demonstrates robust gains across the SE distribution for both moderate and dense user deployments.

Fig. 5 compare the average SE performance of different AP selection schemes for $\tau = 20$, $L = 100$ APs, and $M = 1$ antenna, as the number of users U increases from 20 to 100, thereby capturing the impact of growing user congestion. Across all user loads, the proposed DAPPA scheme achieves the highest SE, starting at approximately 1.05 bit/s/Hz for $U = 20$ and gradually decreasing to around 0.43 bit/s/Hz at $U = 100$. The UG and DCC schemes perform similarly, with DCC slightly outperforming UG at lower U but converging as U increases. SAT and GB consistently yield the lowest SE, with SAT generally performing slightly worse than GB for all U . The performance gap between the proposed scheme and the others is most pronounced for small U (around 7% improvement over the next best at $U = 20$), and although this gap narrows with increasing U , the proposed method retains a noticeable advantage even in high-user scenarios. This trend indicates that while all methods experience performance degradation due to increased inter-user interference and limited pilot resources, the proposed scheme is more resilient, offering superior SE across the entire range of user densities.

Fig. 6 illustrates the impact of the number of pilot sequences τ on the average SE performance of various AP selection techniques, considering $L = 100$ APs, $M = 4$ antennas, $U = 50$ users, and $\tau_c = 200$. Across all τ values, the proposed DAPPA method consistently achieves the highest SE, starting at approximately 1.60 bit/s/Hz for $\tau = 10$ and

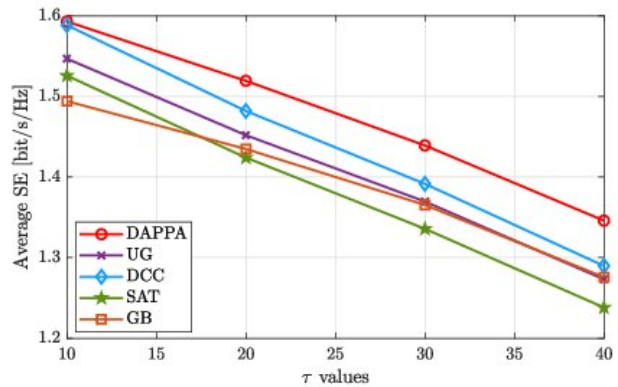


Fig. 6: Average SE performance for different AP selection schemes and the number of pilot sequences with $L = 100$ APs, $M = 4$ antennas, $U = 50$ users, and $\tau_c = 200$

gradually decreasing to about 1.36 bit/s/Hz at $\tau = 40$. The DCC and UG schemes follow closely, with DCC exhibiting slightly better performance than UG for smaller τ values, but converging at larger τ . GB and SAT produce the lowest SE results, with GB marginally outperforming SAT in most scenarios. The performance gap between the proposed method and the others is most pronounced at $\tau = 10$ (approximately 4–6% higher SE compared to DCC and UG) and narrows as τ increases, suggesting that the proposed method gains a greater advantage under shorter pilot sequences, where pilot contamination effects are more severe. All schemes exhibit a monotonic decrease in SE with increasing τ , primarily due to the reduced duration available for data transmission within the coherence interval. The results indicate that the average SE reaches its maximum at $\tau = 10$ for all methods and then declines. This behavior can be explained by the fixed total power per coherence block: distributing this power over longer pilot sequences lowers the per-symbol pilot power, thereby degrading channel estimation accuracy. Furthermore, according to the SE expression $SE = (1 - \frac{\tau}{\tau_c}) \log_2(1 + \text{SINR})$, increasing τ directly reduces the pre-log factor $(1 - \frac{\tau}{\tau_c})$, which in turn lowers the achievable SE.

Fig. 7 compares the impact of the AP configuration on the average uplink throughput of various AP selection schemes, for $U = 50$ and $\tau = 20$. The results reveal a clear upward trend in average uplink throughput with increasing AP count. This improvement can be attributed to the reduced path loss as APs are deployed more densely, along with a gradual decrease in inter-user interference. Across all configurations, the proposed DAPPA scheme consistently outperforms the competing methods, confirming its effectiveness and highlighting its robustness in leveraging additional APs to enhance system throughput.

2) Results based on the power allocation with all APs:

In this subsection, we compare the methods under a setting where only the power allocation scheme is optimized, while all APs are jointly considered. Fig. 8 illustrates the effect of power allocation in the absence of AP selection by showing the SE CDFs of the proposed DAPPA scheme and benchmark methods for two user densities, $U = 40$ and $U = 80$. In both

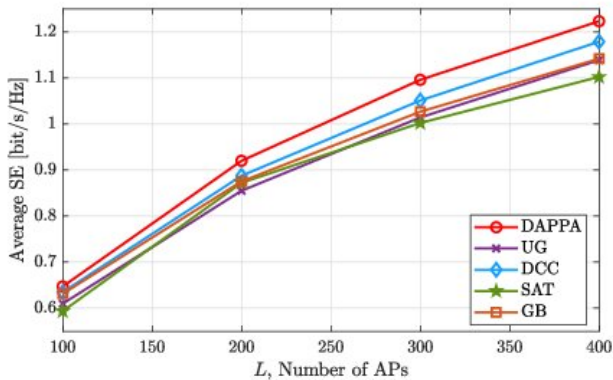


Fig. 7: AP configuration's impact on average SE performance with $\tau = 20$, $U = 50$ user, $M = 1$ antennas, and different number of APs, L

scenarios, the proposed approach consistently shifts the CDF toward higher SE values, indicating improved user fairness and stronger overall performance. The advantage is most pronounced beyond the 95th percentile, where users typically suffer from moderate to poor channel conditions. As the user density increases to $U = 80$, all schemes experience SE degradation due to higher interference and tighter resource constraints; nevertheless, the proposed method preserves a clear performance edge in the mid-percentile region and provides more reliable service to far users. These results demonstrate that the proposed power allocation strategy achieves a more favorable SE distribution than existing optimization-based and learning-based schemes.

Fig. 13 shows the average SE achieved by different pilot

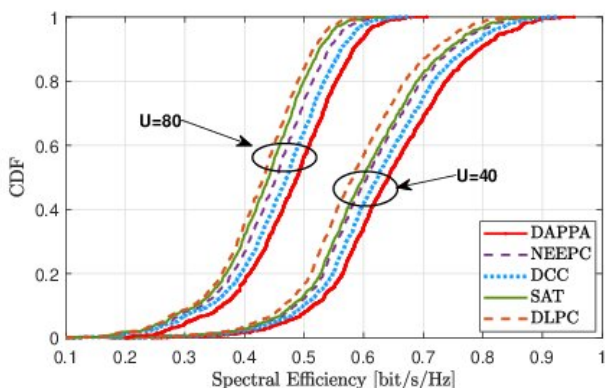


Fig. 8: SE performance in the case with all AP and power allocation are applied to the system with $L = 100$ APs, $M = 1$ antenna, $U = 40$ and 80 users, and $\tau = 20$.

power allocation schemes as a function of the number of users U , assuming that all APs serve all users. The results are shown for a system with $L = 100$ APs, a single antenna per AP ($M = 1$), and pilot length $\tau = 20$. As the number of users increases, the average SE decreases for all schemes due to stronger pilot contamination and increased multi-user interference. Nevertheless, the proposed DAPPA scheme consistently outperforms the benchmark methods across all user

densities. This performance gain highlights the effectiveness of the proposed pilot power allocation in mitigating interference and efficiently utilizing pilot resources. The gap between DAPPA and the other schemes becomes more pronounced as the network becomes more congested, demonstrating the robustness and scalability of the proposed approach in dense user scenarios. Fig. 14 shows the average SE versus the

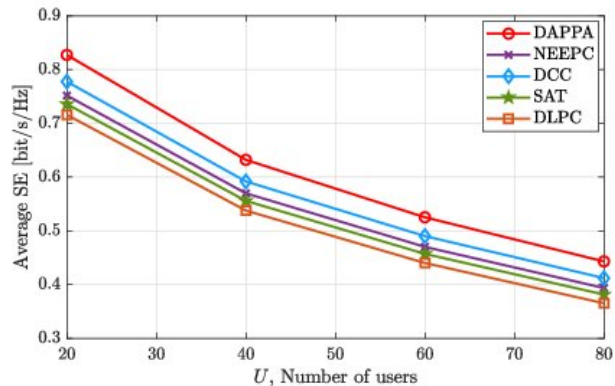


Fig. 9: Performance of schemes with all APs and pilot power allocation for varying numbers of users, with $L = 100$ APs, $M = 1$ antenna, and $\tau = 20$.

pilot length τ for different AP selection and power allocation schemes, considering a system with $L = 100$ APs, a single antenna per AP ($M = 1$), and $U = 40$ users. For all methods, the SE increases for small values of τ , peaks around $\tau \approx 20$, and then gradually decreases as τ grows further. This behavior reflects the fundamental trade-off between pilot contamination and pilot overhead. When τ is small, the reuse of non-orthogonal pilots results in strong pilot contamination and poor channel estimation accuracy. Increasing τ improves pilot orthogonality and estimation quality, leading to higher SE. However, excessively large pilot lengths reduce the portion of the coherence block available for data transmission, which eventually dominates and causes the SE to decline.

Among all schemes, the proposed DAPPA method consistently achieves the highest SE across the entire range of τ values, owing to its effective joint AP selection and power allocation design. At $\tau = 20$, DAPPA reaches a peak SE of approximately 0.648 bit/s/Hz, outperforming the second-best scheme, DCC, by about 5–8%. NEEPC follows closely behind, while SAT exhibits lower performance. DLPC performs the worst for all pilot lengths, indicating its limited capability in interference mitigation and power optimization. Overall, these results emphasize the impact of the pilot length on system performance in CFmMIMO systems and demonstrate that the proposed approach is more resilient in sustaining higher SE across different pilot overhead regimes. Fig. 11 evaluates the fairness performance of the proposed and benchmark schemes from the CDF of the user sum rate. From the CDF in Fig. 11, it can be seen that DAPPA achieves the highest probability of offering larger sum rates compared to all other methods. This gain is attributed to its iterative nature, which balances pilot and data power in every round, thereby mitigating pilot contamination and suppressing inter-user interference more

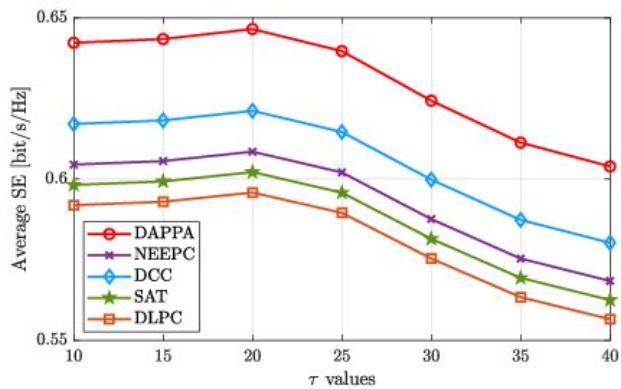


Fig. 10: Average SE performance of different schemes with power allocation for varying τ , with $L = 100$ APs, $M = 1$ antenna, and $U = 40$.

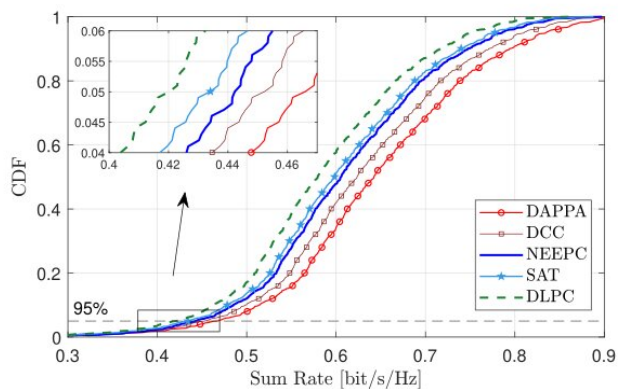
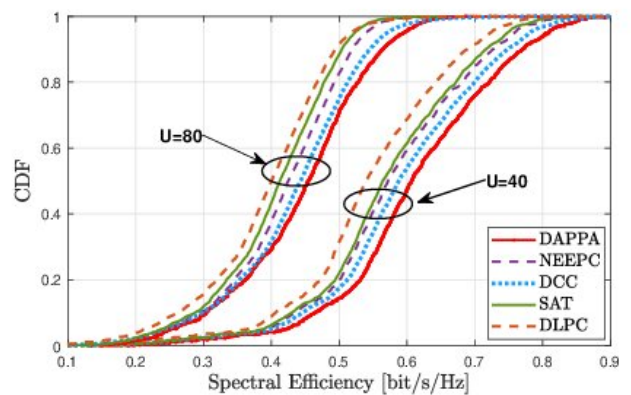


Fig. 11: CDF of sum rate for $\tau = 20$, with $L = 100$ APs, $M = 1$ antenna, and $U = 40$.

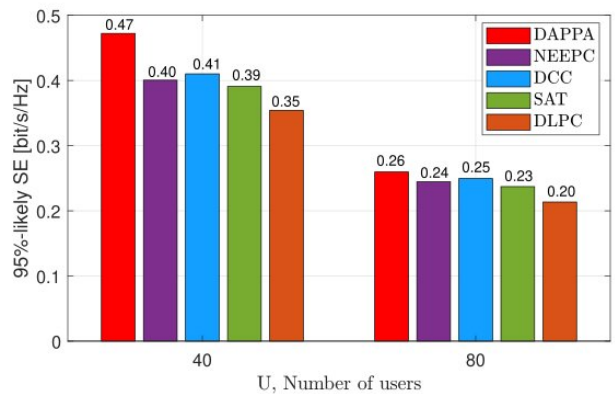
effectively. DCC and NEEPC also yield improved distributions compared to conventional SAT and DLPC, but their tails shift to lower rates, indicating weaker guarantees for the worst-case users.

3) *Results based on the AP selection and the power allocation approach:* In the second subsection, we evaluate the proposed method incorporating both AP selection and power allocation. Its performance is compared against several benchmark schemes: DCC [10], SAT [46], normalized estimation error-based power control (NEEPC) [44], and deep learning-based power control (DLPC) [43].

Fig. 12 depicts the impact of AP selection and the power allocation. Fig. 12a presents the CDF of the SE for the proposed DAPPA method and other benchmark schemes under two user densities, $U = 40$ and $U = 80$. For both cases, the CDF curves for the proposed DAPPA scheme indicate higher SE values for a larger proportion of users. This suggests that the proposed method improves fairness and ensures better average performance across users. The gain is especially visible for more than 80% of the SE distribution, where users typically experience moderate and weak channel conditions. As the network becomes more congested with $U = 80$, the SE for all methods decreases due to increased interference and



(a) CDF of SE



(b) 95% likely SE

Fig. 12: SE performance in the case that the AP selection and power allocation are applied to the system with $L = 100$ APs, $M = 1$ antenna, $U = 40$ and 80 users, and $\tau = 20$.

reduced resource availability; however, the proposed method maintains a noticeable advantage in the mid-percentile range and delivers more robust far user performance compared to the other approaches. These results highlight the proposed power allocation scheme's ability to yield superior SE distribution, outperforming conventional optimization-based and learning-based power control strategies.

Fig. 12b presents the 95%-likely SE for the proposed scheme and other benchmark methods using $L = 100$ APs, $M = 1$ antenna, $\tau = 20$, and two different user counts, $U = 40$ and $U = 80$. For $U = 40$, the proposed DAPPA scheme outperforms the next-best method DCC by approximately 14.6%, while achieving gains of about 17.5% over NEEPC, 20.5% over SAT, and 34.3% over DLPC. When the user count increases to $U = 80$, all schemes experience a significant SE reduction due to increased interference and reduced time-frequency resources; however, the proposed method still maintains an advantage of around 4% over DCC, 8.3% over NEEPC, 13.0% over SAT, and 30.0% over DLPC. These results demonstrate that the proposed approach consistently achieves a higher reliability-oriented SE, with performance gains sustained across both moderate and dense network conditions.

Fig. 13 illustrates the fairness performance evaluation with

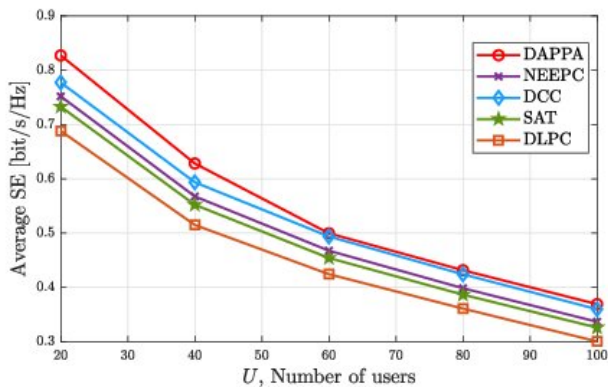


Fig. 13: Performance of AP selection and power allocation schemes for varying numbers of users, with $L = 100$ APs, $M = 1$ antenna, and $\tau = 20$.

the number of users U for the setup of $L = 100$ APs, $M = 1$ antennas, and $\tau = 20$. In all cases, the SE decreases monotonically as the number of users increases, which is expected since more users lead to increased inter-user interference and reduced per-user resource allocation. The proposed DAPPA scheme consistently outperforms all benchmark schemes across the entire user range. At $U = 20$, it achieves the highest SE of approximately 0.83 bit/s/Hz, which is about 10%-15% higher than the best-performing baseline DCC. As U increases, the SE advantage of the proposed method persists, although the gap gradually narrows, reaching around 0.36 bit/s/Hz at $U = 100$. Among the baselines, DCC shows the closest performance to the proposed method, followed by NEEPC and SAT. DLPC consistently yields the lowest SE, indicating that its power control strategy is less effective in managing interference under increasing user density. Notably, the performance difference between NEEPC and SAT is relatively small, especially in high-load scenarios ($U \geq 80$), suggesting similar interference-limited behavior. Overall, it can be seen that the AP selection and power allocation strategies of the proposed method provide a clear performance benefit in both light and heavy load conditions, with the most significant gains observed in the low-to-moderate user regime.

Fig. 14 presents the average SE as a function of the pilot length τ using the AP selection and power allocation schemes, with $L = 100$ APs, $M = 1$ antenna, and $U = 40$ users. Across all schemes, the SE initially increases with τ , reaches a peak around $\tau \approx 15$, and then gradually decreases as τ continues to grow. This trend can be explained as follows: when τ is small, pilot contamination is severe due to non-orthogonal pilot reuse, leading to inaccurate channel estimation. Increasing τ improves pilot orthogonality and channel estimation quality, thus enhancing SE. However, beyond a certain point, a larger τ reduces the fraction of the coherence block available for data transmission, which outweighs the benefit of improved estimation accuracy, causing the SE to decline.

The proposed DAPPA scheme consistently achieves the highest SE across all τ values, benefiting from its AP selection and power allocation strategies. At $\tau = 15$, it attains the

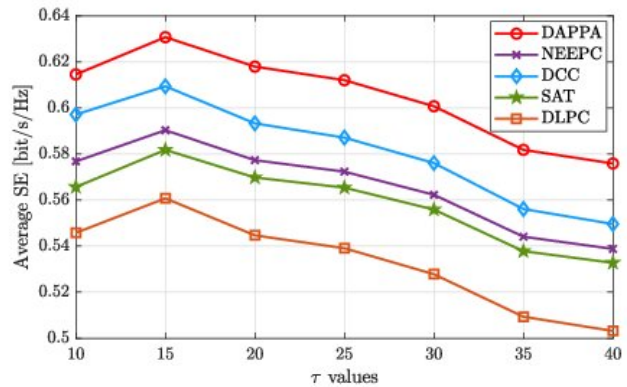


Fig. 14: Average SE performance of different AP selection and power allocation schemes for varying τ , with $L = 100$ APs, $M = 1$ antenna, and $U = 40$.

maximum SE of approximately 0.635 bit/s/Hz, which is about 3-5% higher than the second-best method DCC. NEEPC forms the next performance tier. SAT follows, while DLPC performs the worst for all τ , indicating limited effectiveness in mitigating interference and optimizing power usage. This behavior highlights the trade-off between pilot overhead and channel estimation quality in CFmMIMO, and shows that the proposed method is more robust in maintaining higher SE over the entire range of τ values.

V. CONCLUSION

This paper proposed a dynamic AP selection and pilot power allocation (DAPPA) framework for uplink CFmMIMO systems. Using hierarchical correlation-based clustering, users are associated with APs offering strong channel gains and low correlation, ensuring reliable connectivity, effective interference mitigation, and flexible cluster adjustment without full network reclustering. A user-capacity constraint per AP was introduced to improve scalability, while pilot power allocation was formulated as a WSRM problem and solved iteratively via quadratic transform to enhance SINR and guarantee fairness. Numerical results showed that DAPPA achieves higher spectral efficiency, faster convergence, and robust performance in dense multi-user scenarios compared to benchmark schemes, making it a scalable solution for next-generation CFmMIMO networks.

REFERENCES

- [1] H. Q. Ngo, A. Ashikhmin, H. Yang, E. G. Larsson, and T. L. Marzetta, "Cell-free massive MIMO: Uniformly great service for everyone," in *2015 IEEE 16th international workshop on signal processing advances in wireless communications (SPAWC)*. IEEE, 2015, pp. 201–205.
- [2] —, "Cell-free massive MIMO versus small cells," *IEEE Transactions on Wireless Communications*, vol. 16, no. 3, pp. 1834–1850, 2017.
- [3] M. Bashar, K. Cumanan, A. G. Burr, H. Q. Ngo, M. Debbah, and P. Xiao, "Max-min rate of cell-free massive mimo uplink with optimal uniform quantization," *IEEE Transactions on Communications*, vol. 67, no. 10, pp. 6796–6815, 2019.
- [4] Ö. T. Demir, E. Björnson, L. Sanguinetti *et al.*, "Foundations of user-centric cell-free massive MIMO," *Foundations and Trends® in Signal Processing*, vol. 14, no. 3-4, pp. 162–472, 2021.

- [5] M. Bashar, K. Cumanan, A. G. Burr, M. Debbah, and H. Q. Ngo, "On the uplink max-min SINR of cell-free massive MIMO systems," *IEEE Transactions on Wireless Communications*, vol. 18, no. 4, pp. 2021–2036, 2019.
- [6] M. Bashar, K. Cumanan, A. G. Burr, H. Q. Ngo, E. G. Larsson, and P. Xiao, "Energy efficiency of the cell-free massive mimo uplink with optimal uniform quantization," *IEEE Transactions on Green Communications and Networking*, vol. 3, no. 4, pp. 971–987, 2019.
- [7] C. Hao, T. T. Vu, H. Q. Ngo, M. N. Dao, X. Dang, and M. Matthaiou, "User association and power control in cell-free massive MIMO with the apg method," in *2023 31st European Signal Processing Conference (EUSIPCO)*. IEEE, 2023, pp. 1469–1473.
- [8] B. Chong, H. Lu, L. Qin, Z. Xue, and F. Guo, "Performance optimization on cell-free massive MIMO-aided URLLC systems with user grouping," *IEEE Transactions on Wireless Communications*, 2024.
- [9] E. Björnson and L. Sanguinetti, "Making cell-free massive MIMO competitive with MMSE processing and centralized implementation," *IEEE Transactions on Wireless Communications*, vol. 19, no. 1, pp. 77–90, 2019.
- [10] —, "Scalable cell-free massive MIMO systems," *IEEE Transactions on Communications*, vol. 68, no. 7, pp. 4247–4261, 2020.
- [11] L. Dai, "An uplink capacity analysis of the distributed antenna system (das): From cellular das to das with virtual cells," *IEEE Transactions on Wireless Communications*, vol. 13, no. 5, pp. 2717–2731, 2014.
- [12] Y. Lin, R. Zhang, C. Li, L. Yang, and L. Hanzo, "Graph-based joint user-centric overlapped clustering and resource allocation in ultradense networks," *IEEE Transactions on Vehicular Technology*, vol. 67, no. 5, pp. 4440–4453, 2017.
- [13] H. Q. Ngo, L.-N. Tran, T. Q. Duong, M. Matthaiou, and E. G. Larsson, "On the total energy efficiency of cell-free massive MIMO," *IEEE Transactions on Green Communications and Networking*, vol. 2, no. 1, pp. 25–39, 2017.
- [14] S. Buzzi and C. D'Andrea, "Cell-free massive MIMO: User-centric approach," *IEEE Wireless Communications Letters*, vol. 6, no. 6, pp. 706–709, 2017.
- [15] H. A. Ammar and R. Adve, "Power delay profile in coordinated distributed networks: User-centric v/s disjoint clustering," in *2019 IEEE Global Conference on Signal and Information Processing (GlobalSIP)*. IEEE, 2019, pp. 1–5.
- [16] Y. Lin, R. Zhang, L. Yang, C. Li, and L. Hanzo, "User-centric clustering for designing ultradense networks: Architecture, objective functions, and design guidelines," *IEEE Vehicular Technology Magazine*, vol. 14, no. 3, pp. 107–114, 2019.
- [17] M. Alonzo, S. Buzzi, A. Zappone, and C. D'Elia, "Energy-efficient power control in cell-free and user-centric massive MIMO at mmwave," *IEEE Transactions on Green Communications and Networking*, vol. 3, no. 3, pp. 651–663, 2019.
- [18] S. Chen, J. Zhang, E. Björnson, J. Zhang, and B. Ai, "Structured massive access for scalable cell-free massive MIMO systems," *IEEE Journal on Selected Areas in Communications*, vol. 39, no. 4, pp. 1086–1100, 2020.
- [19] C. Wei, K. Xu, X. Xia, Q. Su, M. Shen, W. Xie, and C. Li, "User-centric access point selection in cell-free massive MIMO systems: A game-theoretic approach," *IEEE Communications Letters*, vol. 26, no. 9, pp. 2225–2229, 2022.
- [20] T. A. Sheikh, S. Deekshitha, N. Shalini, P. Indira, S. Rajasekaran, and J. Borah, "Capacity maximization in cell free massive MIMO network with access point selection method," *International Journal of Sensors Wireless Communications and Control*, vol. 12, no. 9, pp. 661–668, 2022.
- [21] F. Li, Z. Yan, T. Li, Y. Song, and C. Geng, "Access point selection in cell-free mMIMO non-orthogonal multiple access system based on quantum bacterial foraging optimization," vol. 45, no. 6, pp. 2016–2023, 2023.
- [22] J. Wang, L. Dai, L. Yang, and B. Bai, "Clustered cell-free networking: A graph partitioning approach," *IEEE Transactions on Wireless Communications*, vol. 22, no. 8, pp. 5349–5364, 2023.
- [23] S. Mohammadzadeh, S. Mashdour, R. C. de Lamare, K. Cumanan, and C. Li, "Association of access points and users and power allocation for cell-free massive mimo systems," in *2025 IEEE 26th International Workshop on Signal Processing and Artificial Intelligence for Wireless Communications (SPAWC)*. IEEE, 2025, pp. 1–5.
- [24] I. L. Shakya and F. H. Ali, "Joint access point selection and interference cancellation for cell-free massive MIMO," *IEEE Communications Letters*, vol. 25, no. 4, pp. 1313–1317, 2020.
- [25] Z. Duan and F. Zhao, "Pilot allocation and data power optimization based on access point selection in cell-free massive MIMO," *Wireless Communications and Mobile Computing*, vol. 2022, no. 1, p. 4044783, 2022.
- [26] X. Huang, Y. Wang, S. Chen, Y. Li, and Y. Wu, "Joint user clustering and graph coloring based pilot assignment for cell-free massive MIMO systems," *Sensors*, vol. 23, no. 11, p. 5014, 2023.
- [27] M. Yemini and A. J. Goldsmith, "Virtual cell clustering with optimal resource allocation to maximize cellular system capacity," in *2019 IEEE Global Communications Conference (GLOBECOM)*. IEEE, 2019, pp. 1–7.
- [28] J. Bien and R. Tibshirani, "Hierarchical clustering with prototypes via minimax linkage," *Journal of the American Statistical Association*, vol. 106, no. 495, pp. 1075–1084, 2011.
- [29] F. Tan, Q. Deng, and Q. Liu, "Energy-efficient access point clustering and power allocation in cell-free massive MIMO networks: a hierarchical deep reinforcement learning approach," *EURASIP Journal on Advances in Signal Processing*, vol. 2024, no. 1, p. 18, 2024.
- [30] R. Wang, M. Shen, Y. He, and X. Liu, "Performance of cell-free massive MIMO with joint user clustering and access point selection," *IEEE Access*, vol. 9, pp. 40 860–40 870, 2021.
- [31] B. Banerjee, R. C. Elliott, W. A. Krzymień, and M. Medra, "Access point clustering in cell-free massive MIMO using conventional and federated multi-agent reinforcement learning," *IEEE Transactions on Machine Learning in Communications and Networking*, vol. 1, pp. 107–123, 2023.
- [32] S. Mashdour, S. Salehi, R. C. de Lamare, A. Schmeink, and J. P. Lima, "Clustering and scheduling with fairness based on information rates for cell-free MIMO networks," *IEEE Wireless Communications Letters*, 2024.
- [33] R. Mosayebi, M. M. Mojahedian, and A. Lozano, "Linear interference cancellation for the cell-free c-ran uplink," *IEEE Transactions on Wireless Communications*, vol. 20, no. 3, pp. 1544–1556, 2020.
- [34] M. Attarifar, A. Abbasfar, and A. Lozano, "Subset mmse receivers for cell-free networks," *IEEE Transactions on Wireless Communications*, vol. 19, no. 6, pp. 4183–4194, 2020.
- [35] H. Xiao, Y. He, and Z. Hu, "Pilot assignment with graph coloring and power control algorithms in cell-free massive MIMO systems," *Journal of Signal Processing*, vol. 39, no. 7, pp. 1309–1318, 2023.
- [36] E. Björnson, J. Hoydis, M. Kountouris, and M. Debbah, "Massive MIMO systems with non-ideal hardware: Energy efficiency, and capacity limits," *IEEE Transactions on Information Theory*, vol. 60, no. 11, pp. 7112–7139, 2014.
- [37] Y. Zhao, I. G. Niemegeers, and S. H. De Groot, "Power allocation in cell-free massive MIMO: A deep learning method," *IEEE Access*, vol. 8, pp. 87 185–87 200, 2020.
- [38] T. Van Chien, C. Mollén, and E. Björnson, "Large-scale-fading decoding in cellular massive MIMO systems with spatially correlated channels," *IEEE Transactions on Communications*, vol. 67, no. 4, pp. 2746–2762, 2018.
- [39] S. Mohammadzadeh, M. R. Ghourtani, K. Cumanan, A. Burr, and P. Xiao, "Pilot and data power control for scalable uplink cell-free massive mimo," *IEEE Open Journal of the Communications Society*, vol. 6, pp. 10 829–10 844, 2025.
- [40] H. V. Cheng, E. Björnson, and E. G. Larsson, "Optimal pilot and payload power control in single-cell massive MIMO systems," *IEEE Transactions on Signal Processing*, vol. 65, no. 9, pp. 2363–2378, 2016.
- [41] A. Ghazanfari, E. Björnson, and E. G. Larsson, "Optimized power control for massive MIMO with underlaid D2D communications," *IEEE Transactions on Communications*, vol. 67, no. 4, pp. 2763–2778, 2018.
- [42] T. Van Chien, T. N. Canh, E. Björnson, and E. G. Larsson, "Power control in cellular massive MIMO with varying user activity: A deep learning solution," *IEEE Transactions on Wireless Communications*, vol. 19, no. 9, pp. 5732–5748, 2020.
- [43] Y. Zhang, J. Zhang, Y. Jin, S. Buzzi, and B. Ai, "Deep learning-based power control for uplink cell-free massive MIMO systems," in *2021 IEEE global communications conference (GLOBECOM)*. IEEE, 2021, pp. 1–6.
- [44] M. Sarker and A. O. Fapojuwo, "Pilot power allocation scheme for user-centric cell-free massive MIMO systems," in *2023 IEEE 20th Consumer Communications & Networking Conference (CCNC)*. IEEE, 2023, pp. 763–768.
- [45] T. H. Nguyen, T. K. Nguyen, H. D. Han *et al.*, "Optimal power control and load balancing for uplink cell-free multi-user massive MIMO," *IEEE Access*, vol. 6, pp. 14 462–14 473, 2018.
- [46] T. C. Mai, H. Q. Ngo, M. Egan, and T. Q. Duong, "Pilot power control for cell-free massive MIMO," *IEEE Transactions on Vehicular Technology*, vol. 67, no. 11, pp. 11 264–11 268, 2018.
- [47] H. Masoumi and M. J. Emadi, "Joint pilot and data power control in cell-free massive MIMO system," in *2018 Fifth International Conference on*

- Millimeter-Wave and Terahertz Technologies (MMWaTT)*. IEEE, 2018, pp. 34–37.
- [48] T. C. Mai, H. Q. Ngo, and L.-N. Tran, “Design of pilots and power control in the cell-free massive MIMO uplink,” in *2020 54th Asilomar Conference on Signals, Systems, and Computers*. IEEE, 2020, pp. 831–835.
- [49] I. M. Braga, R. P. Antonioli, G. Fodor, Y. C. Silva, and W. C. Freitas, “Joint pilot and data power control optimization in the uplink of user-centric cell-free systems,” *IEEE Communications Letters*, vol. 26, no. 2, pp. 399–403, 2021.
- [50] G. Liu, H. Deng, X. Qian, W. Zhang, and H. Dong, “Joint pilot and data power control for cell-free massive MIMO IoT systems,” *IEEE Sensors Journal*, vol. 22, no. 24, pp. 24 647–24 657, 2022.
- [51] R. Nikbakht and A. Lozano, “Uplink fractional power control for cell-free wireless networks,” in *ICC 2019-2019 IEEE International Conference on Communications (ICC)*. IEEE, 2019, pp. 1–5.
- [52] S. Chakraborty, Ö. T. Demir, E. Björnson, and P. Giselsson, “Efficient downlink power allocation algorithms for cell-free massive MIMO systems,” *IEEE Open Journal of the Communications Society*, vol. 2, pp. 168–186, 2020.
- [53] M. Bashar, A. Akbari, K. Cumanan, H. Q. Ngo, A. G. Burr, P. Xiao, M. Debbah, and J. Kittler, “Exploiting deep learning in limited-fronthaul cell-free massive mimo uplink,” *IEEE Journal on Selected Areas in Communications*, vol. 38, no. 8, pp. 1678–1697, 2020.
- [54] M. Zaher, Ö. T. Demir, E. Björnson, and M. Petrova, “Learning-based downlink power allocation in cell-free massive MIMO systems,” *IEEE Transactions on Wireless Communications*, vol. 22, no. 1, pp. 174–188, 2022.
- [55] L. Salaün, H. Yang, S. Mishra, and C. S. Chen, “A GNN approach for cell-free massive MIMO,” in *GLOBECOM 2022-2022 IEEE Global Communications Conference*. IEEE, 2022, pp. 3053–3058.
- [56] E. Björnson, J. Hoydis, L. Sanguinetti *et al.*, “Massive MIMO networks: Spectral, energy, and hardware efficiency,” *Foundations and Trends® in Signal Processing*, vol. 11, no. 3-4, pp. 154–655, 2017.
- [57] T. L. Marzetta, E. G. Larsson, H. Yang, and H. Q. Ngo, *Fundamentals of massive MIMO*. Cambridge University Press, 2016.
- [58] F. Göttsch, N. Osawa, T. Ohseki, K. Yamazaki, and G. Caire, “Subspace-based pilot decontamination in user-centric scalable cell-free wireless networks,” *IEEE Transactions on Wireless Communications*, vol. 22, no. 6, pp. 4117–4131, 2022.
- [59] N. Osawa, F. Göttsch, I. Kanno, T. Ohseki, Y. Amano, K. Yamazaki, and G. Caire, “Overloaded pilot assignment with pilot decontamination for cell-free systems,” in *2023 IEEE Wireless Communications and Networking Conference (WCNC)*. IEEE, 2023, pp. 1–6.
- [60] P. C. Weeraddana, M. Codreanu, M. Latva-aho, A. Ephremides, C. Fischione *et al.*, “Weighted sum-rate maximization in wireless networks: A review,” *Foundations and Trends® in Networking*, vol. 6, no. 1–2, pp. 1–163, 2012.
- [61] T. V. Gruzdeva and A. S. Strelakovsky, “On solving the sum-of-ratios problem,” *Applied Mathematics and Computation*, vol. 318, pp. 260–269, 2018.
- [62] K. Shen and W. Yu, “Fractional programming for communication systems—part i: Power control and beamforming,” *IEEE Transactions on Signal Processing*, vol. 66, no. 10, pp. 2616–2630, 2018.
- [63] M. Grant, S. Boyd, and Y. Ye, “Cvx: Matlab software for disciplined convex programming,” 2008.
- [64] M. Chiang, C. W. Tan, D. P. Palomar, D. O’neill, and D. Julian, “Power control by geometric programming,” *IEEE Transactions on Wireless Communications*, vol. 6, no. 7, pp. 2640–2651, 2007.
- [65] S. P. Boyd and L. Vandenberghe, *Convex optimization*. Cambridge university press, 2004.
- [66] H. Liu, J. Zhang, S. Jin, and B. Ai, “Graph coloring based pilot assignment for cell-free massive MIMO systems,” *IEEE Transactions on Vehicular Technology*, vol. 69, no. 8, pp. 9180–9184, 2020.
- [67] P. E. Mogensen and J. Wigard, “Cost action 231: Digital mobile radio towards future generation system, final report.” in *On antenna and frequency diversity in GSM. Capacity study of frequency hopping GSM network*, 1999.
- [68] “Further Advancements for E-UTRA Physical Layer Aspects (Release 9),” 3rd Generation Partnership Project (3GPP), 3GPP Technical Specification TS 36.814, 2017, version 9.2.0.